Caffeine degradation using peroxydisulfate and peroxymonosulfate in the presence of Mn 2 O 3 . Efficiency, reactive species formation and application in sewage treatment plant water

Daqing Jia, Olivier Monfort, Khalil Hanna, Gilles Mailhot, Marcello Brigante

Caffeine degradation using peroxydisulfate and peroxymonosulfate in the presence of Mn_2O_3. Efficiency, reactive species formation and application in sewage treatment plant water

Daqing Jia[1], Olivier Monfort[1,2], Khalil Hanna[3,4], Gilles Mailhot[1], Marcello Brigante[1*]

[1] Université Clermont Auvergne, CNRS, SIGMA Clermont, Institut de Chimie de Clermont-Ferrand, F-63000 Clermont–Ferrand, France.

[2] Comenius University in Bratislava, Faculty of Natural Sciences, Department of Inorganic Chemistry, Ilkovicova 6, Mlynska Dolina, 842 15 Bratislava, Slovakia.

[3] Univ Rennes, Ecole Nationale Supérieure de Chimie de Rennes, UMR CNRS 6226, 11 Allée de Beaulieu, F-35708 Rennes Cedex 7, France.

[4] Institut Universitaire de France (IUF), MESRI, 1 rue Descartes, 75231 Paris, France.

* Corresponding author e-mail: marcello.brigante@uca.fr

Abstract

The crucial role of manganese(III) species in the oxidative and catalytic reactivity of manganese oxides have been widely reported. However, the direct activation of radical precursors by Mn(III) oxides is still a matter of discussion. In this work, the ability of Mn(III)-bearing oxide (Mn_2O_3) for activation of peroxydisulfate (PS) and peroxymonosulfate (PMS) was evaluated and compared using caffeine (CAF) as a model pollutant. Complete CAF removal was achieved with 5 mM of PS or PMS after 8 h of reaction time, whereas 48% of mineralization was obtained after 70 h of reaction when PMS was used as oxidant. Electron paramagnetic resonance spin trapping (EPR) and radical scavenging experiments showed that the sulfate radical ($SO_4^{\bullet-}$) was the dominant radical in the Mn_2O_3/PMS system. In comparison, a non-radical mechanism such as Mn_2O_3 surface-activated PS promoted the removal of CAF in the system of Mn_2O_3/PS. Liquid chromatography coupled to mass spectrometry analyses enabled the detection of main degradation products and the proposition of the CAF degradation pathways. Investigations in the real sewage treatment plant water showed that the decrease of CAF removal observed in wastewater as compared to pure water can be alleviated by increasing the Mn_2O_3 dosage. These findings highlight the great ability of Mn-species in PS or PMS activation in different water matrices, which have important implications for the development of novel wastewater treatment technologies.

Keywords: AOPs; Caffeine; Mn_2O_3; Peroxymonosulfate; Peroxydisulfate; Wastewater

1. Introduction

Advanced oxidation processes (AOPs) constitute a promising technology for the remediation of environmental compartments (Miklos et al., 2018). AOPs are efficient in the removal of harmful and persistent organic pollutants in water due to the generation of strongly reactive species (Deng and Zhao, 2015). Hydroxyl radical ($HO^{\bullet}$) belongs to the reactive oxygen species (ROS) and has a high oxidation potential (E^0 = 2.73 V *vs* NHE (Normal Hydrogen Electrode)) (W. Dong et al., 2019). Similarly, the reactive sulfur species (RSS) such as sulfate radical ($SO_4^{\bullet-}$) (E^0 = 2.6 V *vs* NHE) have also caught the attention of the scientific community due to their efficient oxidation abilities (Sbardella et al., 2020). Generation of ROS and RSS is usually performed through the activation of radical precursors by the catalytic processes, such as direct photolysis (Gabet et al., 2021), homogeneous metal ions activation (Jin et al., 2019), and heterogeneous metal oxides catalysis (Yin et al., 2018). The metal oxides-based heterogeneous AOPs represent one of the most investigated strategies for organic pollutants removal in the laboratory and pilot scales (Jia et al., 2018). Among various metal oxides, iron oxides are by far the most studied metal oxides for reactive radicals generation in water (Pi et al., 2019). However, other metal oxides such as manganese oxides (MnOx) are gaining stronger interests due to their versatile oxidation states (II, III, IV, and VII) (Zhong and Zhang, 2019).

Among the different MnO_x, manganese dioxide (MnO_2) has attracted increasing attention due to its good oxidative and catalytic performance for the elimination of pollutants (Kamagate et al., 2020). For instance, Zhou et al. indicated the efficient degradation of 4-nitrophenol by α- and δ-MnO_2 activated PMS through the generation of $SO_4^{\bullet-}$ and $HO^{\bullet}$ (Zhou et al., 2019). Zhu et al. demonstrated the rapid removal of bisphenol A (BPA) in the β-MnO_2/PS system due to the formation of singlet oxygen ($^1O_2$) (Zhu et al., 2019). Moreover, the influence factors for the good catalytic and oxidative performance of various MnO_2 were

investigated by Huang et al., and the results showed that the efficient oxidation of pollutants by MnO_2 with or without oxidants was attributed to the occurrence of Mn(III) on the surface of MnO_2 (Huang et al., 2019, p. 2, 2018). Therefore, it is believed that the presence of Mn(III) species in MnOx can improve the activation efficiency of PS/PMS. Given the above, the direct activation of PS/PMS by Mn(III) oxides was investigated by previous studies. For example, Xu et al. reported the efficient elimination of p-chloroaniline in the γ-MnOOH/PS system through the formation of active intermediates between γ-MnOOH and PS (Xu et al., 2021). Wang et al. indicated the good reactivity of octahedral Mn_3O_4 on PMS activation for ciprofloxacin degradation due to the presence of high contents of Mn(III), Mn(IV) and hydroxyl groups (-OH) (Wang et al., 2021). Moreover, the degradation of organic pollutants by PMS using synthesized Mn_2O_3 as the catalyst was also reported. For instance, Saputra et al. indicated that Mn_2O_3 compared with MnO, Mn_3O_4, MnO_2 showed the highest reactivity in PMS activation for phenol degradation due to the formation of both $SO_4^{\bullet-}$ and $SO_5^{\bullet-}$ radicals (Saputra et al., 2013). The effect of Mn_2O_3 structures on PMS activation was also investigated by Saputra et al., and the results showed cubic-Mn_2O_3 has higher PMS catalysis efficiency due to its high surface area and surface atoms arrangement (Saputra et al., 2014). These experiments demonstrated well the effect of Mn oxidation states and catalyst structures on the activation of PMS. However, the catalytic mechanism of Mn_2O_3 on PMS is not clear, and some important influence factors for the reactivity of Mn_2O_3 such as solution pH were not investigated. Furthermore, Khan et al. investigated the activation of PS using synthesized Mn_2O_3 and MnO_2 for the degradation of phenol in solution (Khan et al., 2021). The results showed that phenol was efficiently removed in A-Mn_2O_3/PS system due to the generation of singlet oxygen ($^1O_2$). Although the authors adopted different experimental methods to identify the generated reactive species and investigated various influence parameters for the reactivity of A-Mn_2O_3/PS system, it should be noted that the experiments were conducted in the acidic environment (pH~3.2). Moreover, since different reactive species were generated in γ-

MnOOH/PS system under different solution pH (Li et al., 2016), thus it is reasonable to deduce that the type of generated reactive species in the Mn_2O_3/PS system can be influenced by solution pH. However, the authors only studied the generated reactive species in the acidic solution. Therefore, it is meaningful to investigate the mechanism of PS/PMS activation by Mn_2O_3 in the near-neutral solution and evaluate the suitability of the Mn_2O_3 activated PS/PMS system in real polluted waters. Caffeine (CAF) was used as a model of organic contaminants since its adverse effects on aquatic organisms and human beings (Buerge et al., 2003). Moreover, CAF as the emerging contaminant has been widely detected in different water matrices at concentrations ranging from ng/L to µg/L (Li et al., 2020).

In this work, we investigated and compared the ability of Mn_2O_3 to activate PS and PMS under different experimental conditions, i.e. pH, Mn_2O_3 dosage, and radical precursor concentrations. Reactive radical species and non-radical pathways were identified and their contribution to the pollutant removal was quantified using chemical scavenging experiments, electron paramagnetic resonance spectroscopy (EPR) and X-ray photoelectron spectroscopy (XPS). Moreover, the CAF degradation pathway, main degradation products and mineralization efficiency were reported. Finally, the ability of both systems was compared in real sewage treatment plant water, where 80 % of CAF degradation was obtained by the proposed method after 20 hours.

2. Materials and Methods

2.1. Chemicals

All chemicals were reagent-grade (see Text S1 in Supplementary Materials) and used as received. Ultrapure water (Millipore, resistivity 18.2 MΩ cm) was used in the preparation of all solutions.

2.2. Catalyst characterization

The purity of the used Mn_2O_3 sample (Sigma-Aldrich) was confirmed by powder X-ray diffraction (XRD) (Fig. S1). The average oxidation state (AOS) of Mn after reaction was obtained using X-ray photoelectron spectroscopy (XPS). The analysis conditions of XRD and XPS were presented in Text S2.

2.3. Experimental procedures

The chemical reactions were performed in a borosilicate brown bottle in which 100 mL of solution was kept at room temperature (298 ± 2 K) under stirring (700 rpm) to ensure homogeneity. 25 µM of CAF was added to the 100 mL reaction solution containing a certain concentration of Mn_2O_3, then a predetermined amount of oxidants (*i.e.* H_2O_2, PS, PMS, and HSO_3^-) was added to start the reaction. The solution pH was fixed by adding 0.1 M sodium hydroxide and perchloric acid. 2 mL of samples were withdrawn at the predetermined interval times and were filtered (0.20 µm PTFE filter) to remove Mn_2O_3 particles. The reaction was stopped by the addition of 100 µL of methanol (HPLC grade, Sigma-Aldrich) and then the samples were analyzed by HPLC.

To determine the involvement of reactive radical species leading to the degradation of CAF, a kinetic competition study was performed using different radical scavengers such as *tert*-butanol (TBA) and 2-Propanol (2-Pr) to quench hydroxyl radical ($HO^{\bullet}$) and sulfate radical ($SO_4^{\bullet-}$) (Buxton et al., 1988; Clifton and Huie, 1989). Furfuryl alcohol (FFA) was used to trap singlet oxygen ($^1O_2$) (Appiani et al., 2017). The contribution of main radical species to the degradation of CAF was estimated considering the second-order rate constants between the selected radicals and quenchers or CAF (see Table S1). The quenching efficiency was determined as $C_1 \times k_1/(C_1 \times k_1 + C_2 \times k_2)$. Where C_1 was the initial concentration of organic

scavengers and k_1 was the second-order rate constant with selected oxidant species (i.e. $HO^{\bullet}$, $SO_4^{\bullet-}$, or $^1O_2$), C_2 and k_2 were the concentration of CAF and reactivity constant with the oxidant species.

Sewage treatment plant water (STPW) was collected in December 2019 from the urban treatment plant named "3 rivières" in Clermont-Ferrand and used after 0.45 µm filtration using PTFE filter. The main physicochemical characteristics are reported in Table S2.

2.4. Chemical analysis and kinetics

CAF concentration was determined by a high-performance liquid chromatography system (HPLC, Alliance 2695 Waters) equipped with a photodiode array detector (DAD) and C18 column (Agilent Eclipse XDB, 250 × 4.6 mm, 5 µm of particle size). The mobile phase was a mixture of acetonitrile (ACN) and milli-q water acidified with 0.1 % phosphoric acid in gradient eluent mode (V_{ACN} / V_{water} from 20/80 to 70/30 in 6 min). The flow rate was set at 0.8 mL min^{-1} and the detection wavelength of CAF was fixed at 272 nm. The pseudo-first-order rate constant of CAF (k'_{CAF}) was determined from the slope of ln (C/C_0) *vs* time plot, where C_0 and C are the concentration of CAF at time 0 and t respectively. The error bars associated to the degradation constant data represent 3σ, derived from the scattering of the experimental data around the fit curves (intra-series variability).

To investigate the mineralization of CAF, total organic carbon (TOC) analysis (TOC-L CPH CN200, SHIMADZU) was performed.

PS and PMS concentrations were measured using a modified spectrophotometric method (Wacławek et al., 2015). Briefly, 100 µL of PS or PMS sample was first transferred into 5 mL of the mixture of potassium iodide (KI, Sigma-Aldrich) and sodium bicarbonate ($NaHCO_3$, Sigma-Aldrich) to generate iodine (I_2). Then, I_2 further reacted with iodide (I^-) leading to the

formation of complex (I_3^-). Finally, I_3^- was detected using a Varian Cary 3 UV-visible spectrophotometer (Abs at 351 nm) and quantified using a calibration curve.

The identification of radicals was performed by electron paramagnetic resonance spectroscopy (EPR). The X-band cw-EPR spectra (modulation frequency of 100 kHz) were monitored at 293 K with the EMX*plus* spectrometer (Bruker) equipped with the High Sensitivity Probe-head (Bruker) in the small quartz flat cell (Wilmad-LabGlass, WG 808-Q) using 5,5-dimethyl-1-pyrroline *N*-oxide (DMPO, Sigma-Aldrich) and 2,2,6,6-tetramethyl-4-piperidinol (TEMP, Sigma-Aldrich) as the spin trapping agents. Typically, 375 µL of sample was withdrawn and immediately mixed with 125 µL of DMPO (100 mM) or TEMP (100 mM), then the mixture was transferred into an EPR quartz capillary tube (0.5 mm, 100 mm) for measurement. The EPR spectrometer settings were as follows: microwave frequency, ~ 9.87 GHz; microwave power, ~6.87 mW; center field, ~352.7 mT; sweep width, 20 mT; sweep time, 30 s; sample *g*-factors, 2.0; modulation amplitude, 1.0 G. The experimental EPR spectra were analyzed by the WinEPR software (Bruker) and the calculations of spin-Hamiltonian parameters and relative concentrations of individual DMPO-adducts were performed with the EasySpin toolbox working on MatLab® platform (Stoll and Schweiger, 2006).

The identification of CAF transformation intermediates was obtained by an LC-MS system coupled with an ESI ion source (MSD VL). The column was a Phenomenex Kinetex C18 column (2.6 µm × 100 Å; 100 × 2.1 mm) using an initial gradient of 5% ACN and 95% water acidified with 1% formic acid (Sigma-Aldrich), followed by a linear gradient to 95% ACN within 15 min and kept constant during 10 min. The flow rate was 0.2 mL min^{-1} and the injection volume of 10 µL.

3. Results and discussion

3.1. Reactivity of Mn_2O_3 with PS and PMS

The reactivity of Mn_2O_3 with different radical precursors (i.e. H_2O_2, PS, PMS, and HSO_3^-) was investigated. As shown in Fig. 1, the CAF degradation was observed only in the Mn_2O_3 activated PS and PMS (5 mM) systems. Up to 40% of removal extent was observed after 3 h of reaction time in the unbuffered solutions. Although the solution pH dropped to 5.5 ± 0.2 and 2.7 ± 0.2 with the addition of PS and PMS, the purpose of checking the reactivity of Mn_2O_3 with PS and PMS was achieved (Table S3). Moreover, blank and adsorption tests showed that CAF removal by adsorption on Mn_2O_3 or direct oxidation by radical precursors was negligible whatever the investigated pH (Fig. S2 and S3). The formation of radical species and their relative contribution to the CAF degradation were determined by chemical scavenging and EPR experiments. Before starting the scavenging tests, suitable concentrations of scavengers were determined through the calculation of scavenging efficiency with reactive oxygen species (ROS). As shown in Table S4, in the presence of 10 mM of TBA, 10 mM of 2-Pr and 1 mM of FFA, a scavenging efficiency of 97.4, 93.2 and 99.4 % of the corresponding ROS was achieved. Thus, the proposed scavenger concentration was enough to inhibit almost the whole radical reactions. In addition, to verify if the degradation of CAF was originated from the heterogeneous reaction between PS/PMS and Mn_2O_3, the leaching of Mn^{2+} in Mn_2O_3 activated PS/PMS reactions and the homogeneous activation of PS/PMS by Mn^{2+} were studied. As shown in Fig. S4. A negligible Mn^{2+} concentration (~ 1 μM) was determined when 0.4 g L^{-1} of Mn_2O_3 was suspended in solution. Moreover, the degradation efficiency of CAF in the Mn^{2+} activated PS/PMS system was far lower than Mn_2O_3, even the employed concentration of Mn^{2+} was 10-1000 times higher than leached Mn^{2+}. Thus, the removal of CAF was attributed to the activation of PS/PMS by Mn_2O_3.

3.1.1 Reactivity of Mn_2O_3 with PS

In the system of Mn_2O_3/PS, only a negligible effect of TBA and 2-Pr was observed indicating that $HO^{\bullet}$ and $SO_4^{\bullet-}$ were not the main radical species involving in the CAF degradation (Fig. 2A). However, in the presence of 1 mM of FFA, the CAF degradation constant (k'_{CAF}) dropped from 2.4×10^{-3} min^{-1} to 2.6×10^{-5} min^{-1}, corresponding to 99% of inhibition after 8 h (Fig. S5). The inhibition of CAF degradation in the presence of FFA can be due to the quenching of $^1O_2$. To identify whether $^1O_2$ was generated in the Mn_2O_3/PS system, the EPR experiments were conducted using TEMP as the spin trapping agent and no signal corresponding to the formation of TEMPO was observed (Fig. S6), thus indicating the inhibition of CAF degradation by FFA was not related to the scavenging of $^1O_2$. Other reasons can explain the inhibition of CAF by FFA, such as the scavenging of $HO^{\bullet}$, the increased PS consumption, and the occupied reactive sites on the Mn_2O_3 surface (Appiani et al., 2017; Xu et al., 2021; Yang et al., 2018)). The scavenging of $HO^{\bullet}$ was excluded since CAF degradation was not inhibited in the presence of TBA (Fig. 2A) while CAF removal was completely suppressed after the simultaneous addition of 2-Pr and FFA (Fig. S7). Moreover, the PS decomposition due to the reactivity with FFA was negligible (Fig. S8) compared to the reactivity in the presence of PMS (Yang et al., 2018). Therefore, the inhibition of CAF degradation in presence of FFA was attributed to the adsorption of FFA on the surface of Mn_2O_3 and competing with PS ions for the active sites. The results are in agreement with previous studies which reported FFA can affect the surface properties of catalysts (Guan et al., 2017; Xu et al., 2021).

Therefore, a non-radical mechanism of PS activation is proposed and it generally includes the generation of $^1O_2$ (as mentioned just above, this hypothesis is excluded), the surface-activated PS species, or the electron transfer process (Ding et al., 2020). It is worth noting that the electron transfer mechanism in PS activation usually happens when carbon-based materials were used as catalysts (Lee et al., 2015). Therefore, the removal of CAF in

the Mn_2O_3/PS system was attributed to the formation of Mn_2O_3 surface-activated PS. The result is in agreement with previous studies which indicated $^1O_2$ was not generated but the active intermediates formed between PS and catalyst were responsible for the degradation of pollutants (Li et al., 2016; Xu et al., 2021).

To better understand the role of PS, the concentration of PS in different systems was monitored (Fig. 2B). The depletion of PS by CAF alone was negligible, whereas a small amount of PS was consumed by Mn_2O_3 in the absence of CAF. This result indicates that PS was absorbed on the active sites present on the surface of Mn_2O_3. CAF as an electron donor leads to the increased consumption of activated PS since in the Mn_2O_3/PS system the depletion of PS was enhanced. Moreover, the decrease trend of PS was close to that of CAF.

The non-radical mechanism of PS activation was further verified through the measurement of the Mn oxidation state in the Mn_2O_3/PS system. The average oxidation state (AOS) of samples was calculated from the binding energy difference (ΔE) of Mn 3s doublet splitting as following: $AOS = 8.956 - 1.126 \times \Delta E$ (W. Yang et al., 2020). Fig. S9 shows that the AOS of Mn_2O_3 did not change after reaction with PS (AOS ~3.00), indicating the activation of PS by Mn_2O_3 was a non-radical catalytic process.

3.1.2 Reactivity of Mn_2O_3 with PMS

In the PMS-containing system, the presence of TBA and 2-Pr decreased the k'_{CAF} from 6.5×10^{-3} min^{-1} to 4.0×10^{-3} min^{-1} and 7.0×10^{-4} min^{-1}, respectively (Fig. 3A and Fig. S10) indicating the predominant role of $SO_4^{\bullet-}$ compared to $HO^{\bullet}$. PMS can react with both $\equiv Mn^{III}$ (Eq. 1) and $\equiv Mn^{IV}$ (Eq. 2) leading to the formation of $SO_4^{\bullet-}$ and $SO_5^{\bullet-}$ (He et al., 2020). Moreover, $SO_5^{\bullet-}$ self-reaction in water can lead to the formation of $SO_4^{\bullet-}$ (Eq. 3) (Yermakov et al., 1993). Formation of $HO^{\bullet}$ occurs through $SO_4^{\bullet-}$ reaction with water and hydroxide, although the latter reaction is only relevant in alkaline solution (Eqs. 4 and 5) (Hayon et al.,

1972). The generation of $SO_4^{\bullet-}$ and $HO^{\bullet}$ was further identified by EPR experiments. As shown in Fig. 3B, the EPR spectrum represents a superposition of two individual signals (according to the results of the best simulation fit), including the nine-line signal of 5,5-dimethyl-2-oxo-pyrroline-1-oxyl ($^{\bullet}$DMPO-X) with the characteristic spin-Hamiltonian parameters (a_N = 0.732 mT, a_H^{γ}(2H) = 0.406 mT; g = 2.0070 ± 0.0001), which is often produced by over-oxidation of DMPO in the presence of reactive oxygen species (*e.g.* $HO^{\bullet}$ or $^1O_2$) (Fontmorin et al., 2016). The second signal is characterized by the hyperfine coupling constants (a_N = 1.373 mT, a_H^{β} = 1.019 mT, a_H^{γ} = 0.135 mT, a_H^{γ} = 0.073 mT), which correlate well with $^{\bullet}$DMPO-SO_4^{-} spin-adduct with limited stability in aqueous media (Buettner, 1987).

$$\equiv Mn^{III} + HSO_5^- \rightarrow \equiv Mn^{IV} + SO_4^{\bullet-} + OH^- \quad (1)$$

$$\equiv Mn^{IV} + HSO_5^- \rightarrow \equiv Mn^{III} + SO_5^{\bullet-} + H^+ \quad (2)$$

$$SO_5^{\bullet-} + SO_5^{\bullet-} \rightarrow O_2 + 2\ SO_4^{\bullet-} \quad (3)$$

$$SO_4^{\bullet-} + OH^- \rightarrow SO_4^{2-} + HO^{\bullet} \quad (4)$$

$$SO_4^{\bullet-} + H_2O \rightarrow SO_4^{2-} + HO^{\bullet} + H^+ \quad (5)$$

Since the addition of FFA exhibited a strong inhibition effect (~ 85%) on CAF degradation (Fig. S11A), thus, to verify whether the generated $^{\bullet}$DMPO-X was derived from the reaction with $^1O_2$, the EPR experiment was further performed. As shown in Fig. S11B, in the presence of 25 mM of TEMP, a typical TEMPO signal (three-line signal with 1:1:1 intensity ratio) was observed in the presence of PMS alone which can be attributed to the self-decomposition of PMS (X. Yang et al., 2020). In Mn_2O_3/PMS system, the TEMPO signal was approximately equal to the TEMPO intensity from PMS alone, indicating that no further $^1O_2$ was generated in the Mn_2O_3/PMS system. Moreover, the addition of FFA in the Mn_2O_3/PMS system also showed a negligible effect on the intensity of the TEMPO signal. Thus, the formation of $^{\bullet}$DMPO-X in the system of Mn_2O_3/PMS cannot be contributed to $^1O_2$. On the

other side, the generated $HO^{\bullet}$ might be responsible for the formation of $^{\bullet}$DMPO-X, consistent with the observations of Yang et al. (X. Yang et al., 2020).

The decomposition of PMS was further investigated. Fig. S11C shows that PMS can be decomposed by FFA alone, and the depletion efficiency of PMS is higher than Mn_2O_3, suggesting the inhibition of CAF degradation in presence of FFA might be also attributed to the increased consumption of PMS.

Besides, the AOS of Mn in the Mn_2O_3/PMS system was measured, as shown in Fig. S9C. The AOS of Mn_2O_3 was increased to 3.10 after reacting with PMS, suggesting the generation of Mn (IV). It is known that Mn (IV) can oxidize organic pollutants compounds through a heterogeneous electron transfer process (Huang et al., 2019), thus the non-radical degradation of CAF in the Mn_2O_3/PMS system might be related to the formation of Mn (IV).

In summary, different activation mechanisms of PS and PMS by the same Mn_2O_3 were exhibited. In the Mn_2O_3/PS system, the catalyst surface-activated PS molecules were the primary reactive species that are responsible for the degradation of pollutants. This can be attributed to the symmetric structure of PS which facilities the contained O-O bonds binding to Mn_2O_3 surface through the substitution with surface hydroxyl groups (-OH) (Z. Dong et al., 2019; Xu et al., 2021; Zhu et al., 2019). In comparison, the activation of PMS by Mn_2O_3 was mainly processed with the generation of radicals. It can be explained by the fact that the unsymmetric structure of PMS can be easier activated by catalysts, the causes are in agreement with the results of previous research (Anipsitakis and Dionysiou, 2004; Lin et al., 2019, 2014).

3.2. Effect of pH

The CAF removal by Mn_2O_3-mediated activation of PS or PMS was also investigated over a wide range of initial pH (3-8) and degradation pseudo-first order rates were plotted versus pH (Fig. 4). In the presence of PS, k'_{CAF} decreased from 4.7×10^{-3} to 2.6×10^{-4} min^{-1} from pH

3 to 8. It should be noted that the neutral form of CAF predominates over the investigated pH range (pK_a = 10.4). The greater efficiency observed at low pH might result from the favorable electrostatic interactions between positively charged Mn_2O_3 (PZC ~5.9) and PS (Salla et al., 2020). The system Mn_2O_3/PMS exhibited an improved k'_{CAF} with increasing the solution pH from 2.2 × 10^{-3} min^{-1} to 6.4 × 10^{-3} min^{-1}, followed by a decrease to 2.4 × 10^{-3} min^{-1} (Fig. 4). The low efficiency at low pH may come from the impact of H^+ concentration on the reactivity of $SO_4^{\bullet-}$, resulting in the low CAF degradation (Huang et al., 2009). Since the oxidation potential of $HO^{\bullet}$ is lower than $SO_4^{\bullet-}$ under alkaline environments, the transformation from $SO_4^{\bullet-}$ to $HO^{\bullet}$ may explain the low efficiency at high pH values. To further explore this transformation process, the scavenging tests with the addition of TBA and 2-Pr were conducted under various initial solution pH (Fig. S12). The contribution of $HO^{\bullet}$ and $SO_4^{\bullet-}$ in the degradation of CAF was also assessed using Eq. S1 (Text S3). As shown in Fig. S12D, the radical involvement percentage (RI) of $HO^{\bullet}$ after 6 h of CAF degradation first decreased from 10% to 7% and then increased to 34% as the initial solution pH increased from 3 to 8. In the meanwhile, the RI percentage of $SO_4^{\bullet-}$ first increased from 55% to 63% and then decreased to 50%. The results fully and directly demonstrated the transformation between $HO^{\bullet}$ and $SO_4^{\bullet-}$ with the change of solution pH. In summary, neutral or basic conditions are suitable for the activation of PMS by Mn_2O_3, while PS activation by Mn_2O_3 was enhanced in acidic conditions only.

3.3. Effects of Mn_2O_3 and oxidant dosages

The effect of Mn_2O_3 concentration on CAF degradation in presence of PS under initial solution pH 5 was then investigated (Fig. 5A and Fig. S13A). An increase of Mn_2O_3 dosage from 0.05 to 1.0 g L^{-1} led to an increase of k'_{CAF} from 5.4 × 10^{-4} min^{-1} to 4.6 × 10^{-3} min^{-1}. Similarly, the removal of CAF by Mn_2O_3 activated PMS was increased with the increase in Mn_2O_3 concentration (Fig. S13B). This effect can be attributed to the increase of the active

surface area of Mn_2O_3, leading to more active sites for radical precursor activation. It is worth noting that complete removal of CAF was obtained for 1.0 g L^{-1} Mn_2O_3 and 5 mM PMS after 2 h, while 8 h reaction time is required for the Mn_2O_3/PS system. The degradation of CAF (k'_{CAF}) by Mn_2O_3 (1.0 g L^{-1}) with PMS (5 mM) was 3.9×10^{-2} min^{-1}, which results in an 8-fold increase compared to that in Mn_2O_3/PS system (4.6×10^{-3} min^{-1}). Fig. 5B shows the increase of the k'_{CAF} from 1.6×10^{-4} min^{-1} to 4.7×10^{-3} min^{-1} with the increase of PS concentration from 1 to 10 mM. The effects of PMS concentration on CAF degradation in the presence of Mn_2O_3 (0.4 g L^{-1}) were similar, where an increase of k'_{CAF} from 3.5×10^{-4} min^{-1} to 8.5×10^{-3} min^{-1} with increasing PMS concentration from 1 to 10 mM. These enhanced degradations with the increase of radical precursor concentrations ($\leq$ 10 mM) can be attributed to the promotion of the number of reactive radicals as discussed in *section 3.1*.

3.4. CAF degradation pathway and mineralization

The main transformation intermediates of CAF in Mn_2O_3-activated PS and PMS systems were identified by LC-MS analysis. The experimental conditions were: $[Mn_2O_3]_0$ = 0.4 g L^{-1}, [CAF] = 25 μM and [PS] = $[PMS]_0$ = 5 mM, initial solution pH = 5.0 and analysis was performed after 2 hours of reaction. The molecular formulas, structures, retention time, and positive/negative molecular ions (m/z) of intermediates are summarized in Table S5, and the possible degradation pathways of CAF are shown in Fig. 6. CAF was identified at $[M+H]^+$ = 195.08 m/z. The first transformation step was the hydrogen abstraction (C8 position) and then water molecule addition generating an intermediate with a keto-enol equilibrium. Further oxidation steps lead to the formation of product P1 at $[M-H]^-$ = 228.19 m/z. Similar transformation processes in CAF oxidation were reported in the previous study (Lin and Chen, 2016; Qi et al., 2013). Subsequently (pathway 1), the intermediate P2 ($[M+H]^+$ = 202.15 m/z, $[M+H-H_2O]^+$ = 184.13 m/z, and $[M-H]^-$ = 200.13 m/z) generated from the

371 decarboxylation of P1 through the attack of radicals and followed by the addition of hydroxyl
372 group was identified.
373 In pathway 2, the C=C bond of product P1 was attacked by radical species, opening the six-
374 member ring and leading to the formation of two carbonyl groups (-C=O) on the carbon
375 bonding with nitrogen (Rosal et al., 2009; Wang et al., 2017). Then the newly formed
376 carbonyl groups might be further attacked by radicals and the C-N broke leading to the loss of
377 nitrogen derivative (-N-CH_3-COOH) and formation of product P3 ($[M+H]^+$ = 188.13 m/z,
378 $[M+H-H_2O]^+$ = 170.12 m/z and $[M-H]^-$ = 186.11 m/z) (Rosal et al., 2009). The intermediate
379 P4 at $[M+H]^+$ = 174.11 m/z and $[M-H]^-$ = 172.09 m/z were further identified, which was
380 originated from P3 through the demethylation process. It is worth noting that not all the
381 intermediates (P1-P4) were observed in the Mn_2O_3/PMS system and this can be explained by
382 the different types of active radicals generated in Mn_2O_3 activated PS and PMS systems (see
383 Table S5).
384 The mineralization efficiency of Mn_2O_3 + PS and PMS systems was monitored by
385 measuring TOC over reaction time. As shown in Fig. 7, 34% and 48% of TOC degradation
386 were reached in Mn_2O_3-activated PS and PMS system in 70 h, while complete removal of
387 CAF was achieved before 8 h of reaction time (Fig. S14). However, the oxidation process
388 remains active for a long time, over 70 h, suggesting the long-term efficiency of the
389 investigated process.
390
391 **3.5. Degradation efficiency in sewage treatment plant waters (STPW)**
392 To assess the performance and ability of Mn_2O_3 + PS and PMS to degrade CAF in the real
393 water body, the degradation was evaluated in STPW (Total Organic Carbon (TOC) = 39.7 mg
394 C L^{-1}, Inorganic Carbon (IC) = 4.5 mg C L^{-1}, pH = 8.1) and compared to milli-q water system
395 using 0.4 and 1.0 g L^{-1} of Mn_2O_3 (Fig. S15). The degradation efficiency of CAF (DE) was
396 determined from the percentage of CAF degraded after 20 hours of reaction and inhibition in

STPW was observed in all experiments (Fig. 8). Generally, this effect can be attributed to the radical scavenging ability of natural organic matter and inorganic carbon (i.e. hydrogen carbonate ions) of STPW that are recognized to be the main inhibitors of radicals in AOPs (Huang et al., 2018). However, in Mn_2O_3/PS system, the main reactive species are the Mn_2O_3 surface-activated PS. The inhibition of CAF degradation in STPW was mainly attributed to the increased ionic strength (Zhang et al., 2014).

The inhibition effect (IE) of STPW was determined as IE = $\left(1 - {DE_{STPW}}/{DE_{milli-q}}\right) \times 100$, in which DE_{STPW} and $DE_{milli-q}$ were the CAF degradation efficiencies in STPW and milli-q water after 20 hours. It is interesting to note that, in the presence of PS, about 95 % of inhibition was reported using two different Mn_2O_3 concentrations. The results verified again the non-radical mechanism in the Mn_2O_3/PS system and the formation of Mn_2O_3 surface-activated PS. However, a decrease of inhibition effect with the increase of Mn_2O_3 concentration was observed using PMS. The CAF degradation efficiency drops from 88.6 to 33.6 % (IE of 62%) when 0.4 g L^{-1} of Mn_2O_3 was used, while only 20% of inhibition in STPW was determined in the presence of 1.0 g L^{-1}. Increasing in the production of reactive species is expected when a higher amount of solid (higher exposed surface area) is used. This finding highlights the crucial role of Mn in promoting oxidation reactions and suggests that manganese-mediated advanced oxidation processes (Mn-AOPs) could be a promising process for wastewater treatment.

4. Conclusion

Mn_2O_3 exhibited higher activation capability for PS and PMS compared with H_2O_2 and HSO_3^-. CAF degradation in the Mn_2O_3-activated PS and PMS was highly influenced by the initial solution pH. PS was efficiently activated by Mn_2O_3 under acidic pH, while under

neutral or alkaline conditions, environmentally relevant pH values, higher degradation was observed using PMS. Chemical quenching and EPR experiments demonstrated that $HO^{\bullet}$ and $SO_4^{\bullet-}$ were the main radicals generated in the system with PMS. In addition, a non-radical mechanism could contribute to the degradation of CAF in the Mn_2O_3/PS system. The degradation efficiency was tested in real STPW and, despite the inhibition of CAF degradation was observed due to the water constituents (mainly inorganic and organic carbon), the central role of Mn_2O_3 activation for highly reactive species formation was demonstrated in particular when PMS was used (about 80 % of CAF degradation was obtained in STPW after 20 hours). Comparison of obtained results in pure and real STPW indicates that a lower inhibition effect (20 %) was obtained using PMS compared to the PS system. Given the ability of Mn_2O_3 to activate PS and PMS, the manganese-based oxidation processes (Mn-AOPs) reactions can be considered as a promising treatment technology for the removal of organic pollutants in water.

Acknowledgments

This work was supported by the Region Council of Auvergne Rhône Alpes, the "Féderation des Recherches en Environnement" through the CPER "Environment" founded by the Region Auvergne, the French government and the FEDER (European Community), IRP CHINE program "Processes for Environmental Remediation (PER)" and CAP 20–25 I-site project. The authors gratefully acknowledge financial support from China Scholarship Council provided to Daqing Jia (No, 201806920034) to study at the University Clermont Auvergne in Clermont-Ferrand, France. We acknowledge the program PAI (Pack Ambition Recherche) SOLDE from the Region Auvergne Rhône Alpes for the financial support of D.J. in this project. Vlasta Brezová is acknowledged for useful discussion on EPR spectra interpretation.

References

Anipsitakis, G.P., Dionysiou, D.D., 2004. Radical generation by the interaction of transition metals with common oxidants. Environ. Sci. Technol. 38, 3705–3712. https://doi.org/10.1021/es035121o

Appiani, E., Ossola, R., Latch, D.E., Erickson, P.R., McNeill, K., 2017. Aqueous singlet oxygen reaction kinetics of furfuryl alcohol: effect of temperature, pH, and salt content. Environ. Sci.: Proc. Imp. 19, 507–516. https://doi.org/10.1039/C6EM00646A

Buerge, I.J., Poiger, T., Müller, M.D., Buser, H.-R., 2003. Caffeine, an anthropogenic marker for wastewater contamination of surface waters. Environ. Sci. Technol. 37, 691–700. https://doi.org/10.1021/es020125z

Buettner, G.R., 1987. Spin Trapping: ESR parameters of spin adducts 1474 1528V. Free Radical Bio. Med. 3, 259–303. https://doi.org/10.1016/S0891-5849(87)80033-3

Buxton, G.V., Greenstock, C.L., Helman, W.P., Ross, A.B., 1988. Critical review of rate constants for reactions of hydrated electrons, hydrogen atoms and hydroxyl radicals ($\cdot OH/\cdot O^-$) in aqueous solution. J. Phys. Chem. Ref. Data 17, 513–886. https://doi.org/10.1063/1.555805

Clifton, C.L., Huie, R.E., 1989. Rate constants for hydrogen abstraction reactions of the sulfate radical, SO_4^-. Alcohols. Int. J. Chem. Kinet. 21, 677–687. https://doi.org/10.1002/kin.550210807

Deng, Y., Zhao, R., 2015. Advanced oxidation processes (AOPs) in wastewater treatment. Curr. Pollut. Rep. 1, 167–176. https://doi.org/10.1007/s40726-015-0015-z

Ding, Y., Wang, X., Fu, L., Peng, X., Pan, C., Mao, Q., Wang, C., Yan, J., 2020. Nonradicals induced degradation of organic pollutants by peroxydisulfate (PDS) and peroxymonosulfate (PMS): Recent advances and perspective. Sci. Total Environ. 142794. https://doi.org/10.1016/j.scitotenv.2020.142794

Dong, W., Jin, Y., Zhou, K., Sun, S.-P., Li, Y., Chen, X.D., 2019. Efficient degradation of pharmaceutical micropollutants in water and wastewater by FeIII-NTA-catalyzed neutral photo-Fenton process. Sci. Total Environ. 688, 513–520. https://doi.org/10.1016/j.scitotenv.2019.06.315

Dong, Z., Zhang, Q., Chen, B.-Y., Hong, J., 2019. Oxidation of bisphenol A by persulfate via Fe_3O_4-α-MnO_2 nanoflower-like catalyst: Mechanism and efficiency. Chem. Eng. J. 357, 337–347. https://doi.org/10.1016/j.cej.2018.09.179

Fontmorin, J.M., Burgos Castillo, R.C., Tang, W.Z., Sillanpää, M., 2016. Stability of 5,5-dimethyl-1-pyrroline-N-oxide as a spin-trap for quantification of hydroxyl radicals in processes based on Fenton reaction. Water Res. 99, 24–32. https://doi.org/10.1016/j.watres.2016.04.053

Gabet, A., Métivier, H., de Brauer, C., Mailhot, G., Brigante, M., 2021. Hydrogen peroxide and persulfate activation using UVA-UVB radiation: Degradation of estrogenic compounds and application in sewage treatment plant waters. J. Hazard. Mater. 405, 124693. https://doi.org/10.1016/j.jhazmat.2020.124693

Guan, C., Jiang, J., Pang, S., Luo, C., Ma, J., Zhou, Y., Yang, Y., 2017. Oxidation kinetics of bromophenols by nonradical activation of peroxydisulfate in the presence of carbon nanotube and formation of brominated polymeric products. Environ. Sci. Technol. 51, 10718–10728. https://doi.org/10.1021/acs.est.7b02271

Hayon, E., Treinin, A., Wilf, J., 1972. Electronic spectra, photochemistry, and autoxidation mechanism of the sulfite-bisulfite-pyrosulfite systems. SO_2^-, SO_3^-, SO_4^-, and SO_5^- radicals. J. Am. Chem. Soc. 94, 47–57. https://doi.org/10.1021/ja00756a009

He, D., Li, Y., Lyu, C., Song, L., Feng, W., Zhang, S., 2020. New insights into MnOOH/peroxymonosulfate system for catalytic oxidation of 2,4-dichlorophenol: Morphology dependence and mechanisms. Chemosphere 255, 126961. https://doi.org/10.1016/j.chemosphere.2020.126961

Huang, J., Dai, Y., Singewald, K., Liu, C.-C., Saxena, S., Zhang, H., 2019. Effects of MnO_2 of different structures on activation of peroxymonosulfate for bisphenol A degradation under acidic conditions. Chem. Eng. J. 370, 906–915. https://doi.org/10.1016/j.cej.2019.03.238

Huang, J., Zhong, S., Dai, Y., Liu, C.-C., Zhang, H., 2018. Effect of MnO_2 Phase Structure on the Oxidative reactivity toward bisphenol A degradation. Environ. Sci. Technol. 52, 11309–11318. https://doi.org/10.1021/acs.est.8b03383

Huang, Y.-H., Huang, Y.-F., Huang, C., Chen, C.-Y., 2009. Efficient decolorization of azo dye reactive black B involving aromatic fragment degradation in buffered Co^{2+}/PMS oxidative processes with a ppb level dosage of Co^{2+}-catalyst. J. Hazard. Mater. 170, 1110–1118. https://doi.org/10.1016/j.jhazmat.2009.05.091

Jia, D., Sun, S.-P., Wu, Z., Wang, N., Jin, Y., Dong, W., Chen, X.D., Ke, Q., 2018. TCE degradation in groundwater by chelators-assisted Fenton-like reaction of magnetite: Sand columns demonstration. J. Hazard. Mater. 346, 124–132. https://doi.org/10.1016/j.jhazmat.2017.12.031

Jin, Y., Wang, X., Sun, S.-P., Dong, W., Wu, Z., Bian, G., Wu, W.D., Chen, X.D., 2019. Hydroxyl and sulfate radicals formation in UVA/Fe^{III}-NTA/$S_2O_8^{2-}$ system: Mechanism and effectiveness in carbamazepine degradation at initial neutral pH. Chem. Eng. J. 368, 541–552. https://doi.org/10.1016/j.cej.2019.02.182

Kamagate, M., Pasturel, M., Brigante, M., Hanna, K., 2020. Mineralization enhancement of pharmaceutical contaminants by radical-based oxidation promoted by oxide-bound metal Ions. Environ. Sci. Technol. 54, 476–485. https://doi.org/10.1021/acs.est.9b04542

Khan, A., Zhang, K., Sun, P., Pan, H., Cheng, Y., Zhang, Y., 2021. High performance of the A-Mn_2O_3 nanocatalyst for persulfate activation: Degradation process of organic contaminants via singlet oxygen. J. Colloid Interf. Sci. 584, 885–899. https://doi.org/10.1016/j.jcis.2020.10.021

Lee, H., Lee, H.-J., Jeong, J., Lee, J., Park, N.-B., Lee, C., 2015. Activation of persulfates by carbon nanotubes: Oxidation of organic compounds by nonradical mechanism. Chem. Eng. J. 266, 28–33. https://doi.org/10.1016/j.cej.2014.12.065

Li, S., Wen, J., He, B., Wang, J., Hu, X., Liu, J., 2020. Occurrence of caffeine in the freshwater environment: Implications for ecopharmacovigilance. Environ. Pollut. 263, 114371. https://doi.org/10.1016/j.envpol.2020.114371

Li, Y., Liu, L.-D., Liu, L., Liu, Y., Zhang, H.-W., Han, X., 2016. Efficient oxidation of phenol by persulfate using manganite as a catalyst. J. Mol. Catal. A: Chem. 411, 264–271. https://doi.org/10.1016/j.molcata.2015.10.036

Lin, H., Li, S., Deng, B., Tan, W., Li, R., Xu, Y., Zhang, H., 2019. Degradation of bisphenol A by activating peroxymonosulfate with $Mn_{0.6}Zn_{0.4}Fe_2O_4$ fabricated from spent Zn-Mn alkaline batteries. Chem. Eng. J. 364, 541–551. https://doi.org/10.1016/j.cej.2019.01.189

Lin, H., Wu, J., Zhang, H., 2014. Degradation of clofibric acid in aqueous solution by an EC/Fe^{3+}/PMS process. Chem. Eng. J. 244, 514–521. https://doi.org/10.1016/j.cej.2014.01.099

Lin, K.-Y.A., Chen, B.-C., 2016. Efficient elimination of caffeine from water using Oxone activated by a magnetic and recyclable cobalt/carbon nanocomposite derived from ZIF-67. Dalton Trans. 45, 3541–3551. https://doi.org/10.1039/C5DT04277A

Miklos, D.B., Remy, C., Jekel, M., Linden, K.G., Drewes, J.E., Hübner, U., 2018. Evaluation of advanced oxidation processes for water and wastewater treatment – A critical review. Water Res. 139, 118–131. https://doi.org/10.1016/j.watres.2018.03.042

Pi, Z., Li, X., Wang, D., Xu, Q., Tao, Z., Huang, X., Yao, F., Wu, Y., He, L., Yang, Q., 2019. Persulfate activation by oxidation biochar supported magnetite particles for tetracycline removal: Performance and degradation pathway. J. Clean. Prod. 235, 1103–1115. https://doi.org/10.1016/j.jclepro.2019.07.037

Qi, F., Chu, W., Xu, B., 2013. Catalytic degradation of caffeine in aqueous solutions by cobalt-MCM41 activation of peroxymonosulfate. Appl. Catal. B: Environ. 134–135, 324–332. https://doi.org/10.1016/j.apcatb.2013.01.038

Rosal, R., Rodríguez, A., Perdigón-Melón, J.A., Petre, A., García-Calvo, E., Gómez, M.J., Agüera, A., Fernández-Alba, A.R., 2009. Degradation of caffeine and identification of the transformation products generated by ozonation. Chemosphere 74, 825–831. https://doi.org/10.1016/j.chemosphere.2008.10.010

Salla, J.S., Padoin, N., Amorim, S.M., Li Puma, G., Moreira, R.F.P.M., 2020. Humic acids adsorption and decomposition on Mn_2O_3 and α-Al_2O_3 nanoparticles in aqueous suspensions in the

presence of ozone. J. Environ. Chem. Eng. 8, 102780. https://doi.org/10.1016/j.jece.2018.11.025
Saputra, E., Muhammad, S., Sun, H., Ang, H.-M., Tadé, M.O., Wang, S., 2014. Shape-controlled activation of peroxymonosulfate by single crystal α-Mn_2O_3 for catalytic phenol degradation in aqueous solution. Appl. Catal. B: Environ. 154–155, 246–251. https://doi.org/10.1016/j.apcatb.2014.02.026
Saputra, E., Muhammad, S., Sun, H., Ang, H.-M., Tadé, M.O., Wang, S., 2013. Manganese oxides at different oxidation states for heterogeneous activation of peroxymonosulfate for phenol degradation in aqueous solutions. Appl. Catal. B: Environ. 142–143, 729–735. https://doi.org/10.1016/j.apcatb.2013.06.004
Sbardella, L., Velo Gala, I., Comas, J., Morera Carbonell, S., Rodríguez-Roda, I., Gernjak, W., 2020. Integrated assessment of sulfate-based AOPs for pharmaceutical active compound removal from wastewater. J. Clean. Prod. 260, 121014. https://doi.org/10.1016/j.jclepro.2020.121014
Stoll, S., Schweiger, A., 2006. EasySpin, a comprehensive software package for spectral simulation and analysis in EPR. J. Magn. Reson. 178, 42–55. https://doi.org/10.1016/j.jmr.2005.08.013
Wacławek, S., Grübel, K., Černík, M., 2015. Simple spectrophotometric determination of monopersulfate. Spectrochim. Acta 149, 928–933. https://doi.org/10.1016/j.saa.2015.05.029
Wang, F., Xiao, M., Ma, X., Wu, S., Ge, M., Yu, X., 2021. Insights into the transformations of Mn species for peroxymonosulfate activation by tuning the Mn_3O_4 shapes. Chem. Eng. J. 404, 127097. https://doi.org/10.1016/j.cej.2020.127097
Wang, J., Sun, Y., Jiang, H., Feng, J., 2017. Removal of caffeine from water by combining dielectric barrier discharge (DBD) plasma with goethite. J. Saudi Chem. Soc. 21, 545–557. https://doi.org/10.1016/j.jscs.2016.08.002
Xu, X., Zhang, Y., Zhou, S., Huang, R., Huang, S., Kuang, H., Zeng, X., Zhao, S., 2021. Activation of persulfate by MnOOH: Degradation of organic compounds by nonradical mechanism. Chemosphere 272, 129629. https://doi.org/10.1016/j.chemosphere.2021.129629
Yang, W., Peng, Y., Wang, Ya, Wang, Yun, Liu, H., Su, Z., Yang, Weinan, Chen, J., Si, W., Li, J., 2020. Controllable redox-induced in-situ growth of MnO_2 over Mn_2O_3 for toluene oxidation: Active heterostructure interfaces. Appl. Catal. B: Environ. 278, 119279. https://doi.org/10.1016/j.apcatb.2020.119279
Yang, X., Wang, X., Li, Y., Wu, Z., Wu, W.D., Chen, X.D., Sun, J., Sun, S.-P., Wang, Z., 2020. A bimetallic Fe–Mn oxide-activated oxone for in situ chemical oxidation (ISCO) of trichloroethylene in groundwater: Efficiency, sustained activity, and mechanism investigation. Environ. Sci. Technol. 54, 3714–3724. https://doi.org/10.1021/acs.est.0c00151
Yang, Y., Banerjee, G., Brudvig, G.W., Kim, J.-H., Pignatello, J.J., 2018. Oxidation of organic compounds in water by unactivated peroxymonosulfate. Environ. Sci. Technol. 52, 5911–5919. https://doi.org/10.1021/acs.est.8b00735
Yermakov, A.N., Zhitomirsky, B.M., Poskrebyshev, G.A., Sozurakov, D.M., 1993. The branching ratio of peroxomonosulfate radicals (SO_5^-) self-reaction aqueous solution. J. Phys. Chem. 97, 10712–10714. https://doi.org/10.1021/j100143a031
Yin, R., Sun, J., Xiang, Y., Shang, C., 2018. Recycling and reuse of rusted iron particles containing core-shell Fe-FeOOH for ibuprofen removal: Adsorption and persulfate-based advanced oxidation. J. Clean. Prod. 178, 441–448. https://doi.org/10.1016/j.jclepro.2018.01.005
Zhang, T., Chen, Y., Wang, Y., Le Roux, J., Yang, Y., Croué, J.-P., 2014. Efficient peroxydisulfate activation process not relying on sulfate radical generation for water pollutant degradation. Environ. Sci. Technol. 48, 5868–5875. https://doi.org/10.1021/es501218f
Zhong, S., Zhang, H., 2019. New insight into the reactivity of Mn(III) in bisulfite/permanganate for organic compounds oxidation: The catalytic role of bisulfite and oxygen. Water Res. 148, 198–207. https://doi.org/10.1016/j.watres.2018.10.053
Zhou, Z.-G., Du, H.-M., Dai, Z., Mu, Y., Tong, L.-L., Xing, Q.-J., Liu, S.-S., Ao, Z., Zou, J.-P., 2019. Degradation of organic pollutants by peroxymonosulfate activated by MnO_2 with different

crystalline structures: Catalytic performances and mechanisms. Chem. Eng. J. 374, 170–180. https://doi.org/10.1016/j.cej.2019.05.170

Zhu, S., Li, X., Kang, J., Duan, X., Wang, S., 2019. Persulfate activation on crystallographic manganese oxides: Mechanism of singlet oxygen evolution for nonradical selective degradation of aqueous contaminants. Environ. Sci. Technol. 53, 307–315. https://doi.org/10.1021/acs.est.8b04669

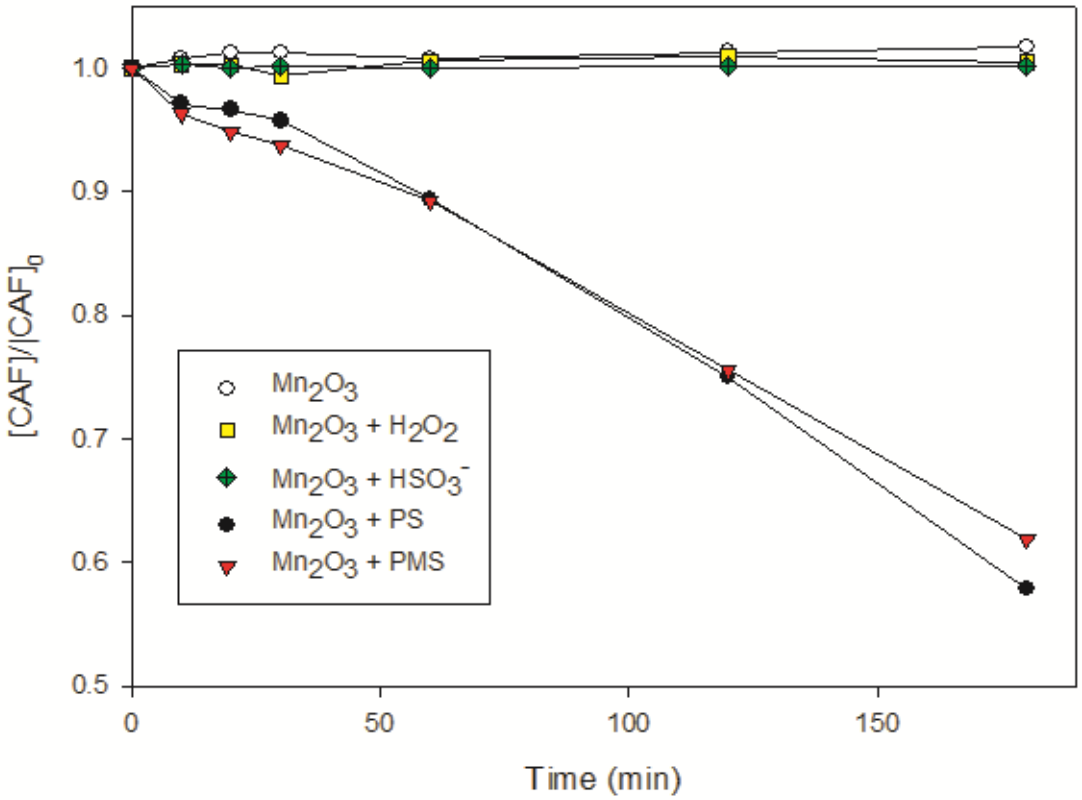

609

610 **Fig. 1.** CAF (25 µM) degradation in the presence of 0.4 g L^{-1} of Mn_2O_3 and different oxidants

611 at 5 mM, natural pH (see Table S2), and T = 298 K.

612

613

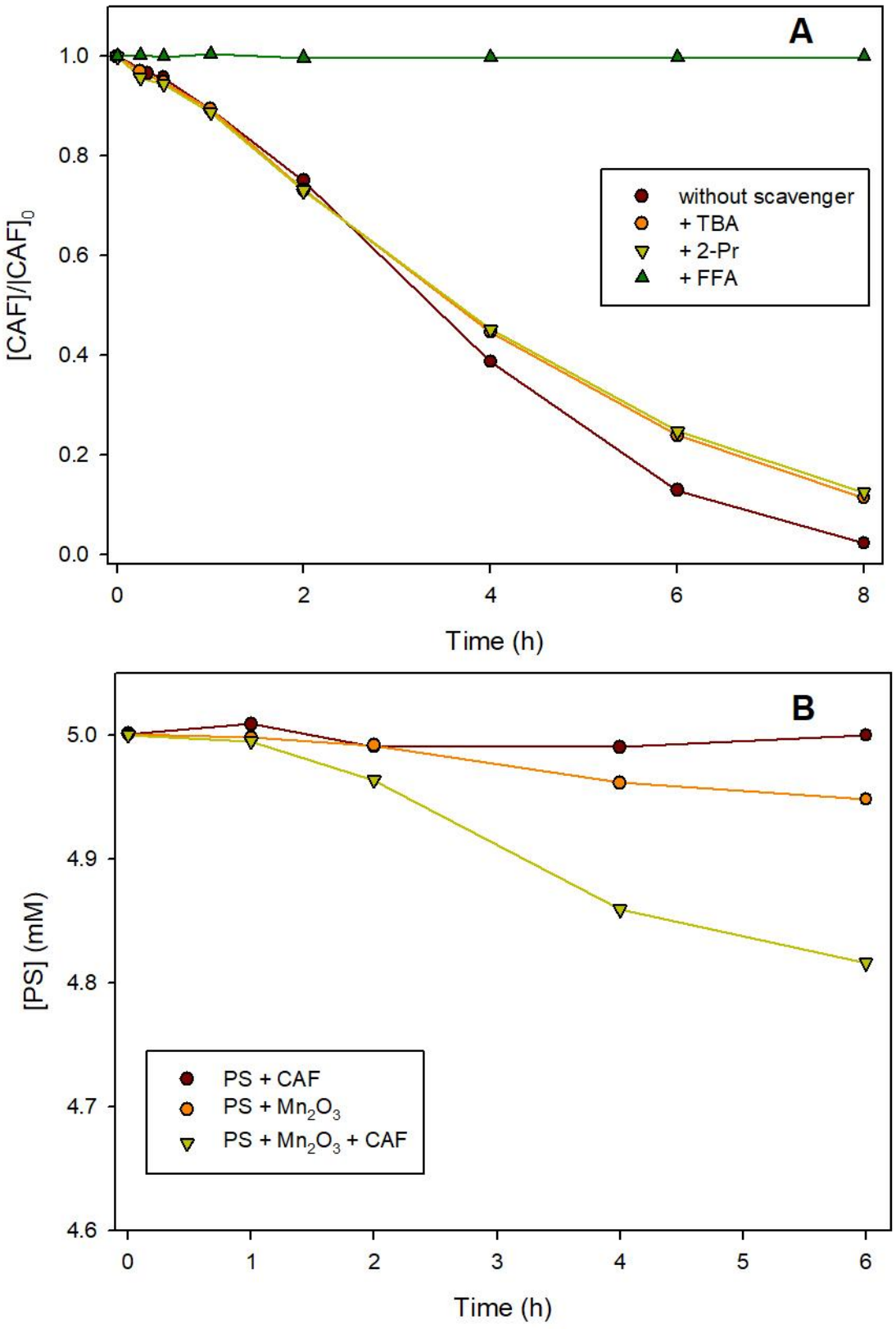

614

615 **Fig. 2.** Determination of ROS species for CAF oxidation in Mn_2O_3/PS. **A:** CAF degradation

616 by Mn_2O_3 with PS in the presence of different radical scavengers ($[TBA]_0 = [2\text{-}Pr]_0$ = 10 mM,

617 $[FFA]_0$ = 1 mM). **B:** PS decomposition in different processes. $[Mn_2O_3]_0$ = 0.4 g L^{-1}, $[CAF]_0$ =

618 25 µM, $[PS]_0$ = 5 mM, The pH of solution was 5.0 and T = 298 K.

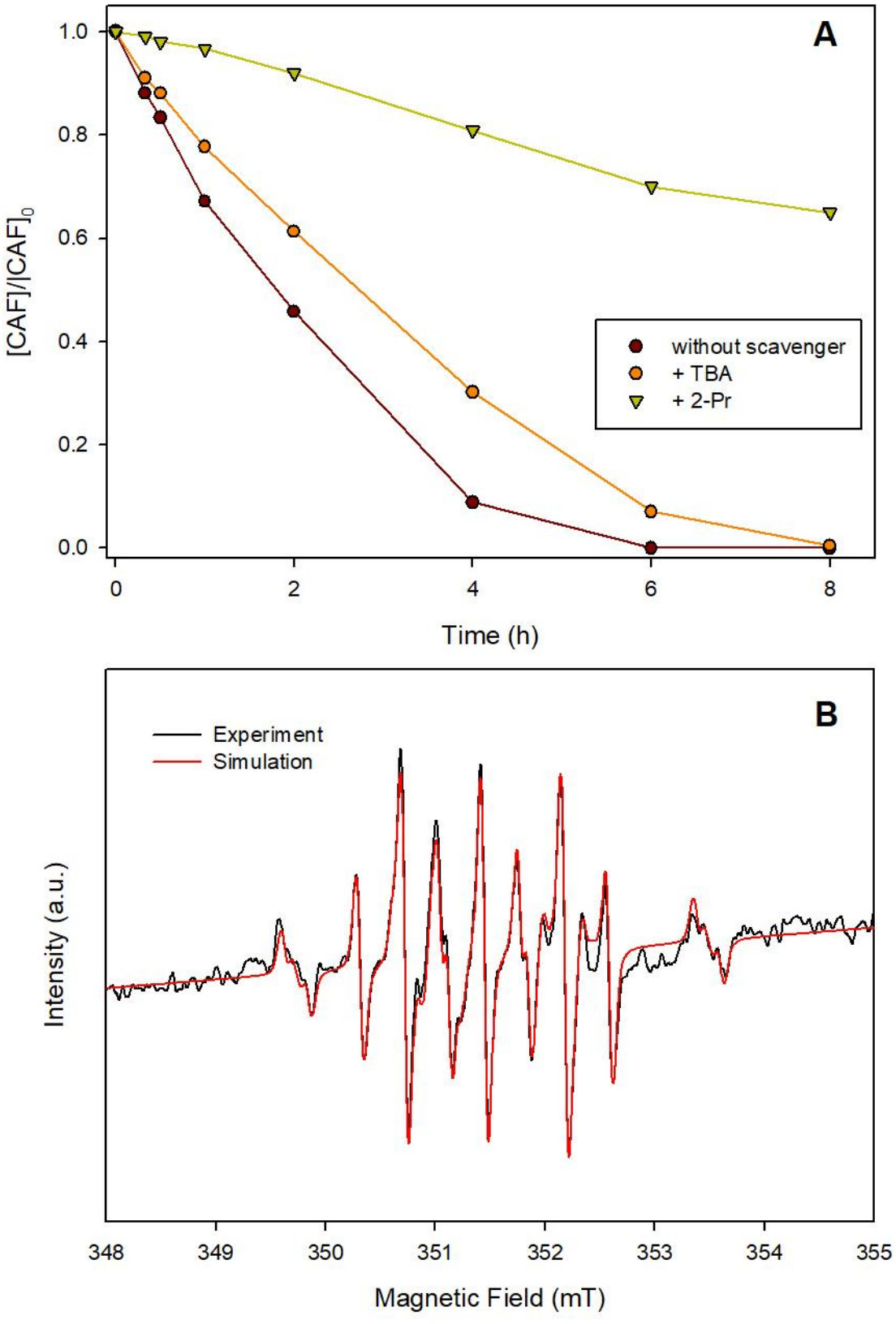

619

Fig. 3. Determination of reactive radical species for CAF degradation in Mn_2O_3/PMS system. **A:** Quenching tests of CAF degradation in the process of Mn_2O_3 + PMS with various radical scavengers ($[TBA]_0$ = $[2\text{-Pr}]_0$ = 10 mM, $[FFA]_0$ = 1 mM). **B:** The normalized experimental (black line) and simulated (red line) EPR spectra measured in the suspension of PMS/Mn_2O_3/DMPO/water ($[DMPO]_0$ = 25 mM). $[Mn_2O_3]_0$ = 0.4 g L^{-1}, $[CAF]_0$ = 25 µM, $[PMS]_0$ = 5 mM, The pH of solution was 5.0 and T = 298 K.

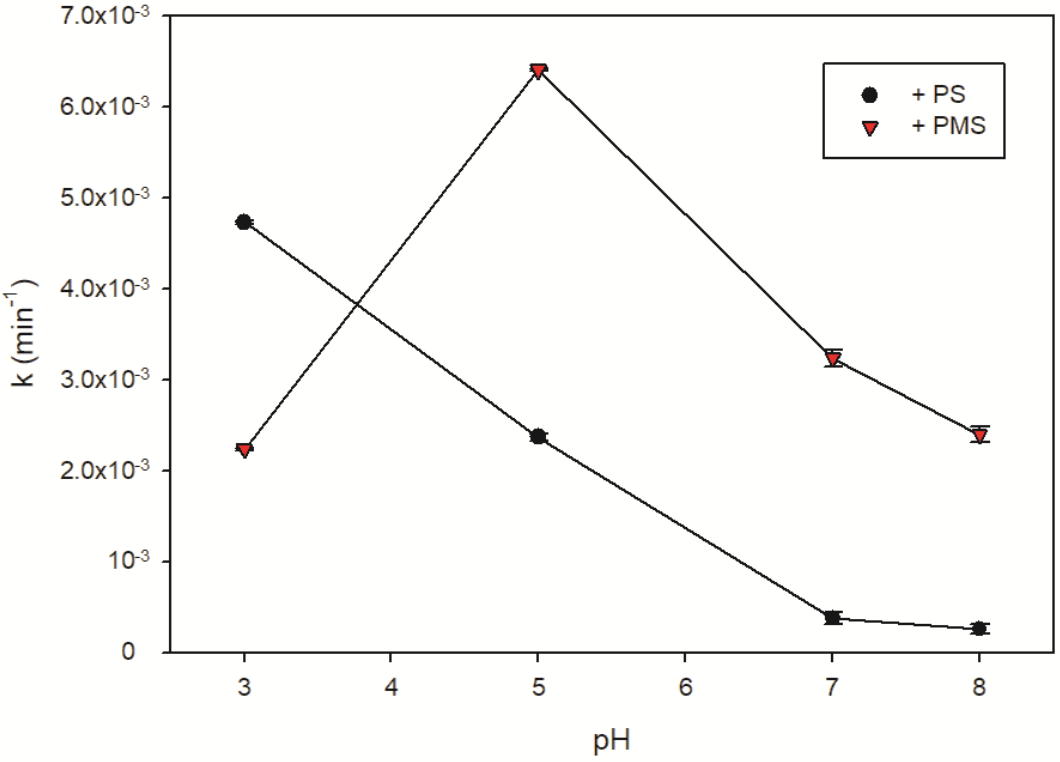

Fig. 4. Degradation constant of CAF (k'CAF) in the systems Mn_2O_3 + PS and Mn_2O_3 + PMS under different pH values. Experimental conditions are $[Mn_2O_3]_0$ = 0.4 g L^{-1}, $[CAF]_0$ = 25 µM, $[PS]_0$ = $[PMS]_0$ = 5 mM, T = 298 K.

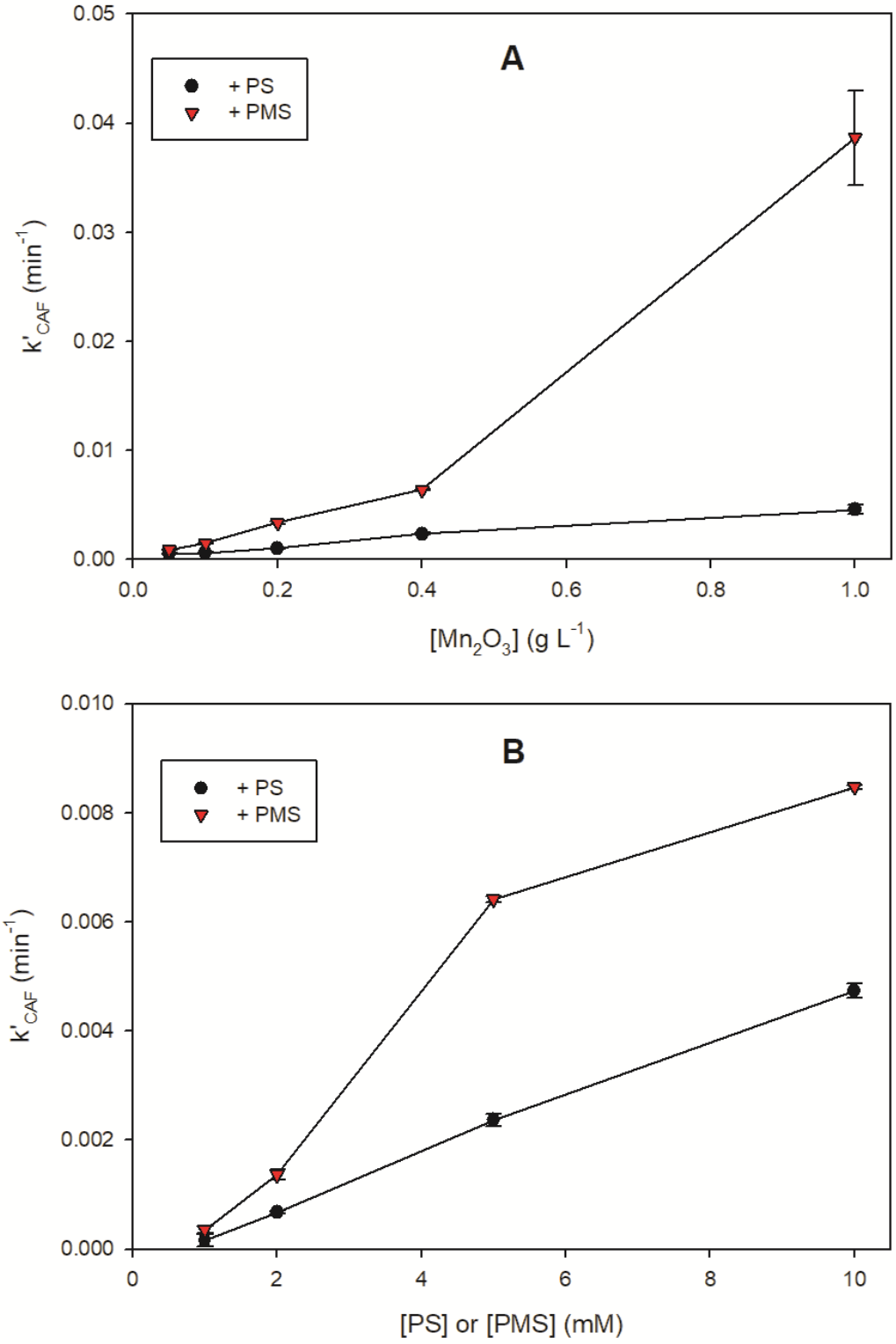

631

632 **Fig. 5.** Degradation of CAF (k'CAF) in the system Mn_2O_3 with PS and PMS. **A:** Effect of

633 Mn_2O_3 concentration in the presence of 5 mM PS and PMS. **B:** Effect of PS and PMS

634 concentrations using 0.4 g L^{-1} of Mn_2O_3. Initial pH = 5.0, T = 298 K.

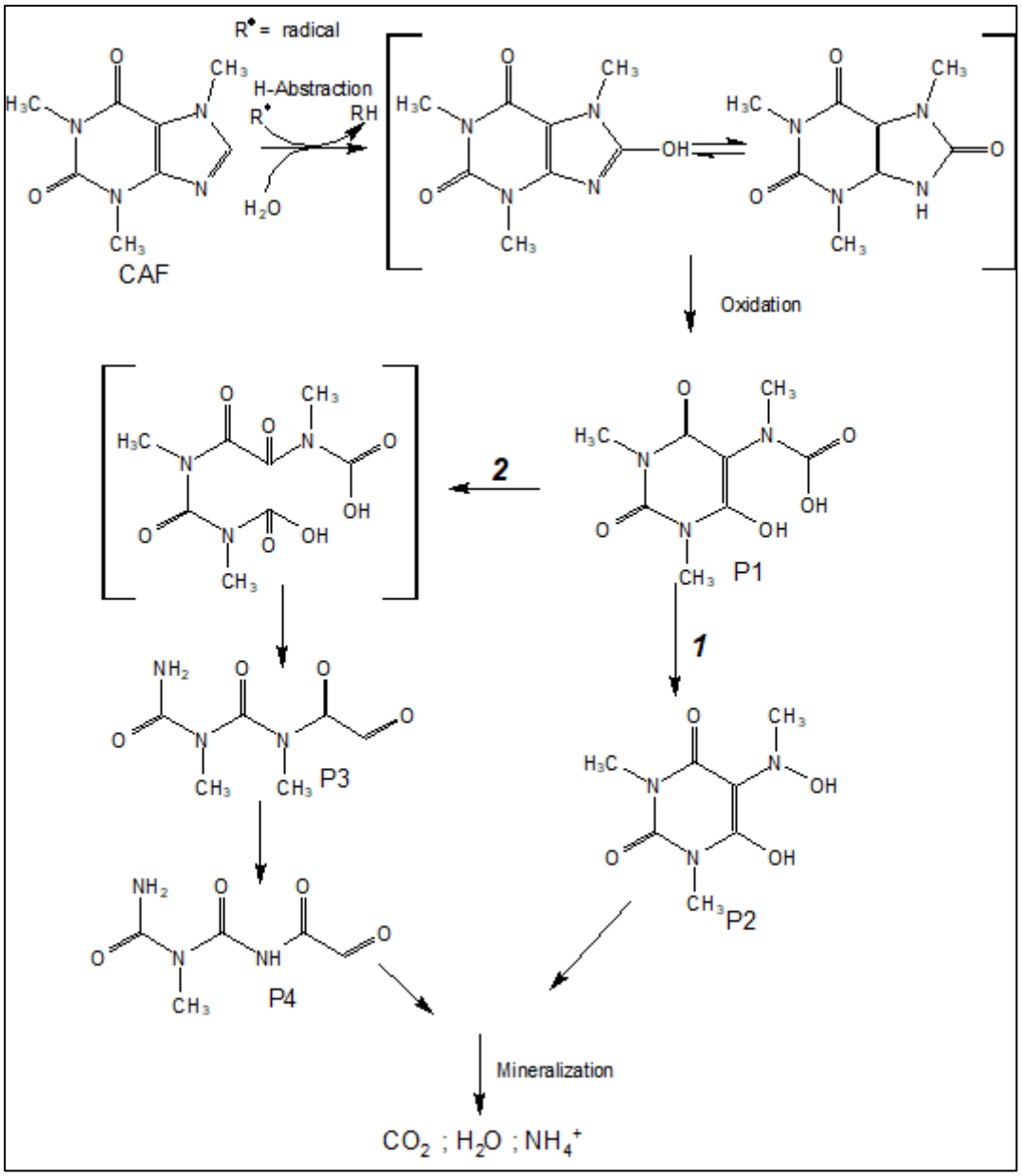

635

636 **Fig. 6.** Proposed degradation pathways of CAF in Mn_2O_3-activated PS and PMS systems. P2

637 and P4 were identified only in the presence of PS (see table S5).

638

639

640

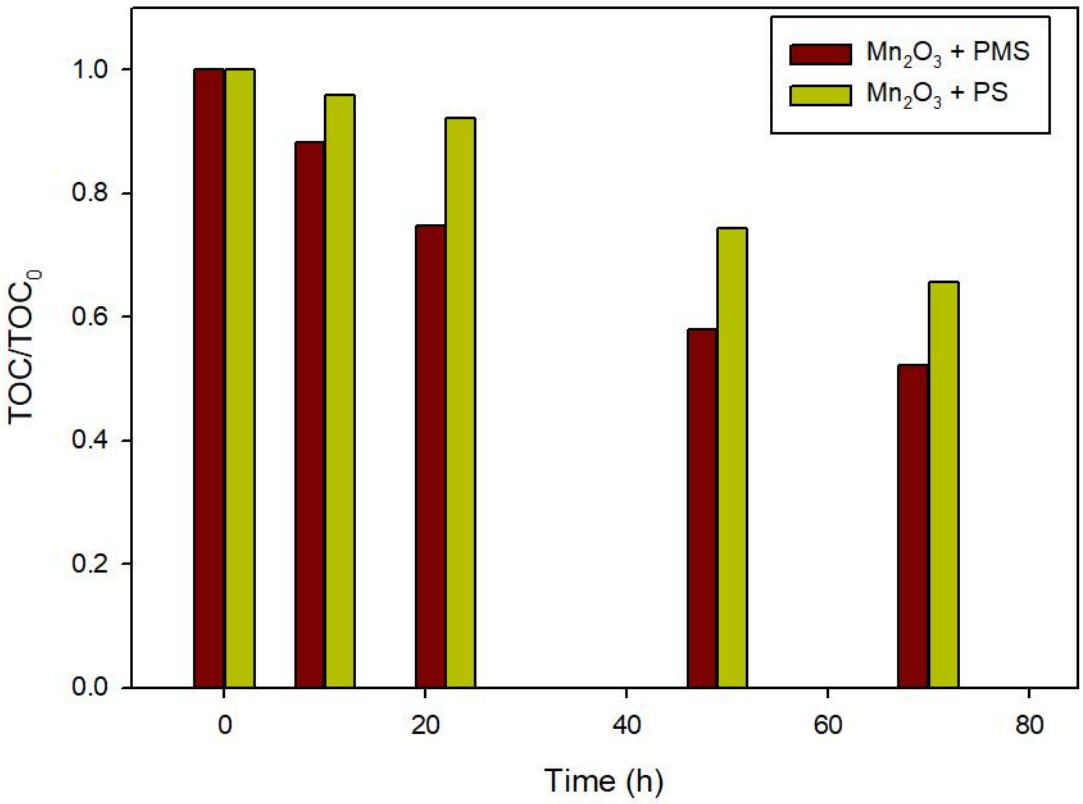

641

642 **Fig. 7.** TOC decrease with time in Mn_2O_3-activated PS and PMS systems. Experimental

643 conditions: $[Mn_2O_3]_0$ = 0.4 g L^{-1}, $[CAF]_0$ = 25 µM, $[PS]_0 = [PMS]_0$ = 5 mM, initial solution

644 pH = 5.0, T = 25 ± 2 °C.

645

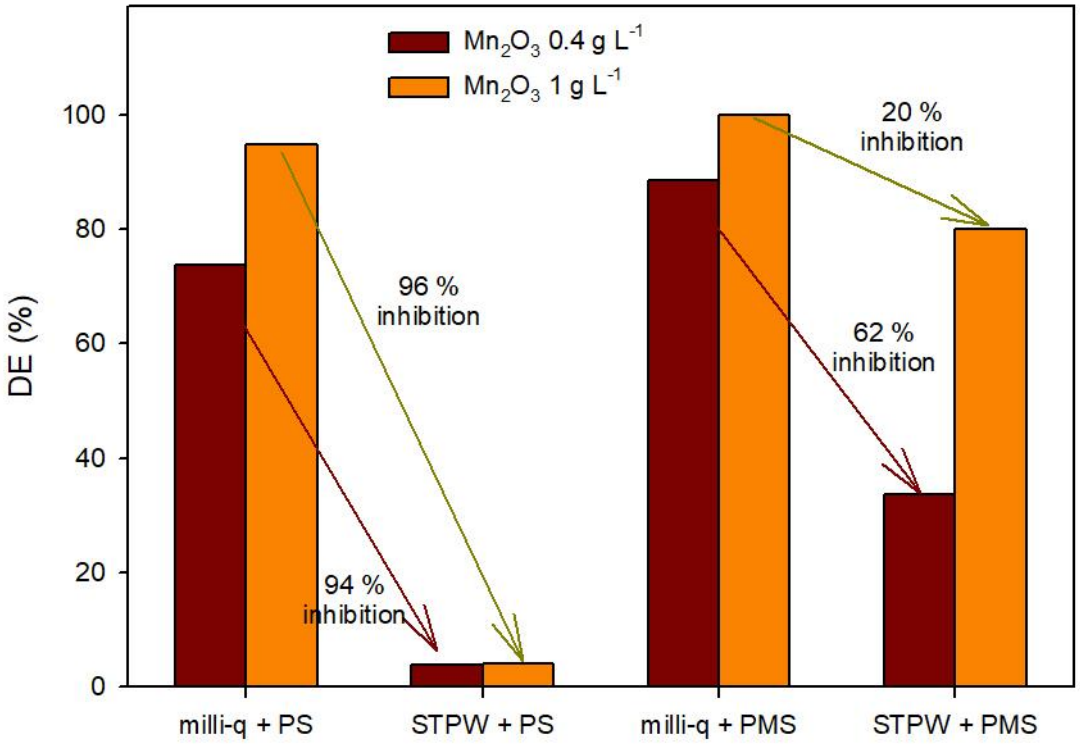

646

647 **Fig. 8.** The degradation efficiency of CAF after 20 hours of reaction in milli-q and STP

648 waters (STPW) using 0.4 and 1.0 g L^{-1} of Mn_2O_3. PS and PMS concentrations were 5 mM and

649 the pH of solutions was 8.0 ± 0.2.